Journal of Marine Research, 44, 93–118, 1986

Stirring and mixing of thermohaline anomalies

by A. Colin de Verdiere,[1] J. G. Harvey[2] and M. Arhan[1]

ABSTRACT

Data from the Tourbillon Experiment in the eastern North Atlantic indicate clearly the stirring of waters with contrasting thermohaline properties by a mesoscale eddy, and the ensuing mixture which occurred. The observed features are discussed in relation to a mixing scenario which considers the salinity distribution in the eastern N. Atlantic associated with the Mediterranean Water (MW) outflow through the Straits of Gibraltar to provide a large-scale context. A mesoscale eddy near the boundary of this water mass advected and deformed a blob of MW, sharpening thermohaline fronts so that double diffusive frontal intrusions developed. Double diffusion processes are invoked as the basic mixing mechanism between the contrasting waters, and following the model of Joyce the lateral mesoscale diffusivity across these fronts is estimated to be 4 $m^2 s^{-1}$. Estimates are made of the lateral fluxes to sub-eddy scales (<20 km) by a number of essentially independent approaches, viz: (a) evaluating the changes in the temperature, salinity and potential vorticity of a particular patch of water, the successive positions of which are deduced from daily optimal streamfunction charts constructed from direct current measurements; (b) evaluating the rate of increase of salinity of the "inner shell" of the eddy which is attributed to mixing with the more saline "outer shell," (c) considering the warm salty blob of MW which was drawn into the eddy circulation as a dye patch and determining its rate of spreading from the increase of its radially symmetrical variance. All of these approaches indicate downgradient mixing of temperature, salinity and potential vorticity anomalies with effective lateral diffusivity of the order of 10^2 $m^2 s^{-1}$. This is considered to be a shear-augmented diffusivity. Using a salinity flux deduced from the eddy heat fluxes computed from the 8-month moored current meter data together with the large-scale salinity gradient implies large-scale diffusivities of the order 5×10^2 $m^2 s^{-1}$; these summarize the averaged effect of many eddy events and can be used to parameterize lateral mesoscale eddy fluxes. It is shown that salt fluxes of the magnitude estimated are of the order required to balance the input of salt through the Straits of Gibraltar and maintain the large-scale salinity distribution in the eastern North Atlantic.

1. Introduction

There have been several attempts during the last fifteen years to fit together the various mechanisms occurring at different scales in the mixing of oceanic thermohaline anomalies. Studying mixing at water mass boundaries, Joyce (1977) showed how the combined action of interleaving and small-scale vertical mixing could act to maintain

1. IFREMER/Centre de Brest, BP 337, 29273 Brest Cedex, France.
2. School of Environmental Sciences, University of East Anglia, Norwich, England NR4 7TJ.

sharp thermohaline fronts. Although that author indicates, in his conclusion, that frontal meandering and subsequent pinching off of a large volume of one water mass into another may be another efficient mode of transfer, he does not introduce any mesoscale contribution to mixing in his model. The role played by eddies in the dispersal of tracer anomalies is taken into account by Garrett (1982), who considers them a necessary ingredient to locally enhance the large-scale thermohaline gradients, after which a scenario similar to that of Joyce can operate, based on frontal intrusions and double diffusion as a small-scale vertical mixing mechanism.

Considering more specifically the part played by eddy-induced horizontal shear, Rhines and Young (1983) following Okubo (1967) and Batchelor (1959) have described theoretically how the tracer gradients first increase under the effect of horizontal shear and are then rapidly smoothed along streamlines, with mixing across streamlines occurring on a longer time scale. The release of a tracer spot in a two-dimensional turbulent field has also been carried out numerically by Haidvogel and Keffer (1984).

During an intensive mesoscale survey in the eastern North Atlantic, the Tourbillon experiment, an anticyclonic eddy was discovered and monitored for about two months commencing September 1979, using CTD measurements, moored current-meters, and subsurface floats. Although the main objective of the experiment was a dynamical study of mesoscale structures in that oceanic region, the location where the eddy was found proved to be on the boundary of the large-scale Mediterranean Water (MW) plume, so that the observations of temperature and salinity could be used as an illustration of the various mixing mechanisms evoked above. The present paper is devoted to this "mixing" aspect of the experiment. Le Groupe Tourbillon (1983) (hereafter LGT) noted that the main eddy entrained and deformed a warm salty MW patch initially present to the south of it. Although Arhan and Colin de Verdiere (1985) suggested that the behavior of the eddy may have been influenced by dynamical effects associated with the MW blob, this intrusion is viewed here as a purely passive tracer. Estimates are given of the horizontal diffusion coefficients characteristic of each scale of motion, with an attempt, based on the models quoted above, to rationalize their relative values. Special emphasis is placed here on the crucial role of eddies and their shear-augmented effects. The different scales are defined in Section 2. A global scenario for the mixing of the large scale MW anomaly is proposed, whose successive steps are developed in the three following sections, starting from the basic small-scale processes (Section 3), then the eddy action (Section 4), and ending with some large-scale speculations (Section 5).

2. Scale definitions

a. The large-scale context. The intermediate salinity maximum in vertical profiles in the eastern N. Atlantic associated with the spreading of the MW outflow typically occurs at a density $\sigma_\theta \sim 27.6$ and has a value $\gtrsim 35.5‰$. Hence the salinity on this

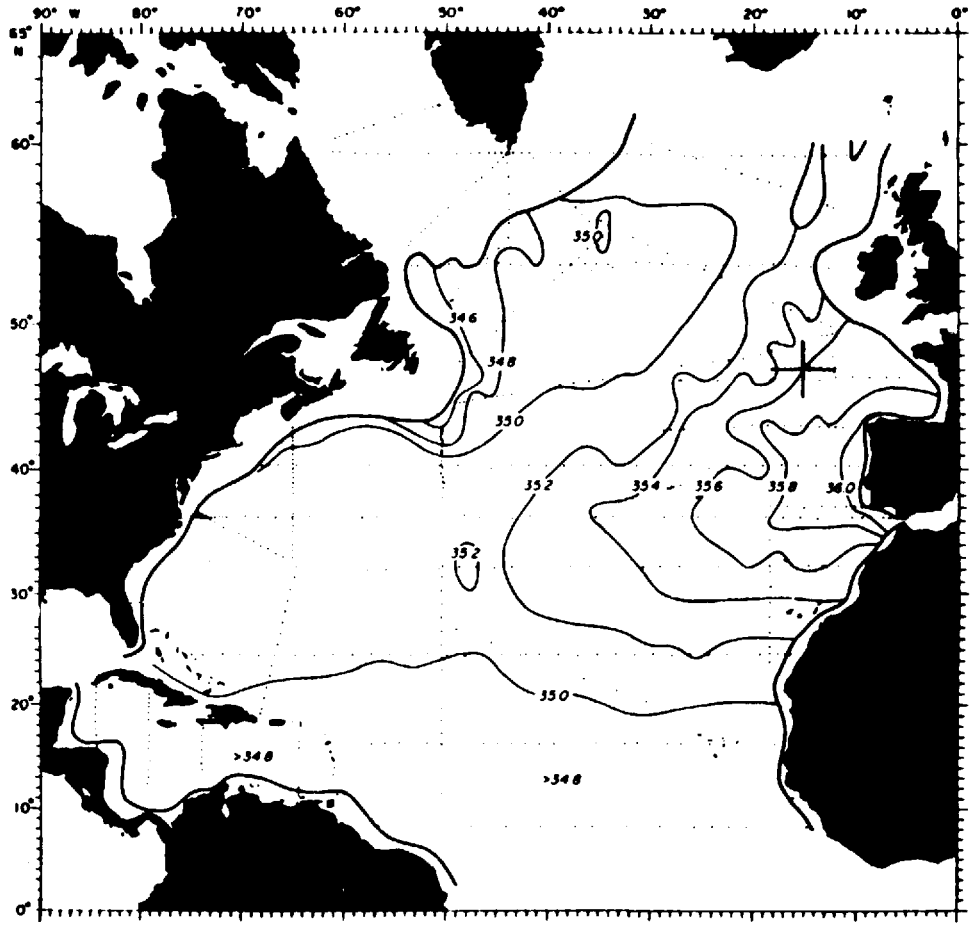

Figure 1. Salinity on the 27.6 σ_θ surface in the North Atlantic from McDowell (1982). The cross indicates the center of the Tourbillon area (47N, 15W).

isopycnal (Fig. 1, from McDowell, 1982) provides a good indication of the location and extent of the large-scale MW plume. The Tourbillon area, shown on the figure by a cross, appears to be located in the large-scale MW salinity gradient and close to the boundary of the region where an intermediate salinity maximum is to be expected.

The position of this water mass boundary is confirmed when focussing on the (200 × 200) km^2 Tourbillon area (Fig. 2). The main mesoscale signal at 1000 db in the four hydrographic (CTD) arrays of the experiment is that of an anticyclonic eddy intensified above the main pycnocline (850 db) (Fig. 2a). A blob of water of Mediterranean origin, recognizable through its salinity signature in Figure 2b, is present in the southern quadrant in array 1, and is subsequently advected and deformed by the mesoscale eddy. Also shown in Figure 2c is the total quasi-geostrophic potential

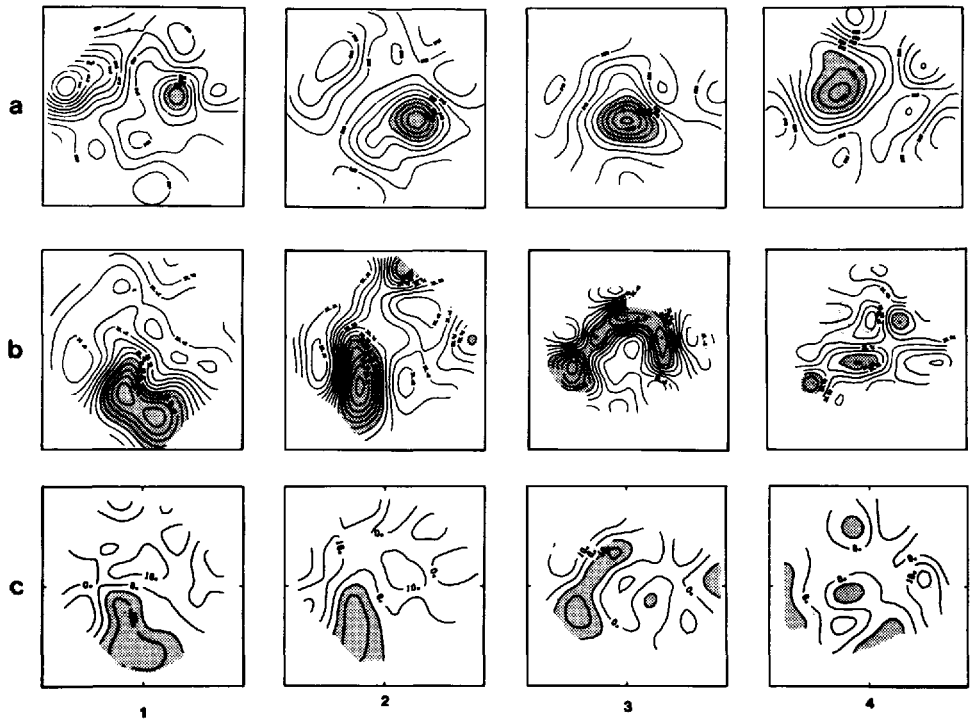

Figure 2. (a) Topography (in db) of the isopycnal surface $\sigma_1 = 32.0$ (shaded area >960 db). (b) Salinity on the isopycnal surface $\sigma_1 = 32.0$. (shaded area >35.62‰); (c) Potential vorticity at 1000 db. (shaded area $<10 \times 10^{-6}$ rad s^{-1}). The fields are shown at the times of the four CTD arrays: 6 Sept., 22 Sept., 4 Oct., 15 Oct., 1979.

vorticity field (relative vorticity and planetary vorticity and vortex stretching) computed using optimal estimation techniques by Arhan and Colin de Verdiere (1985). A negative potential vorticity anomaly appears to be closely related to the MW positive salt anomaly in the successive arrays, an indication of the "tracer nature" of the former which will be used in this paper. The signature in potential vorticity of our MW tracer implies a dynamic role discussed by Arhan and Colin de Verdiere (1985). This must be kept in mind when applying the results of this paper to other truly passive tracers.

b. The eddy action. The evolution of the MW tracer being sheared and advected around the eddy by velocities of order 10 cm s^{-1}, is well illustrated in Figure 2. Between arrays 1 and 3, the mesoscale velocity field is teasing out the MW anomaly, reducing its width but not having much influence on its intensity, so that a sharpening of the transverse thermohaline gradients may be observed. After array 3 a fragmentation

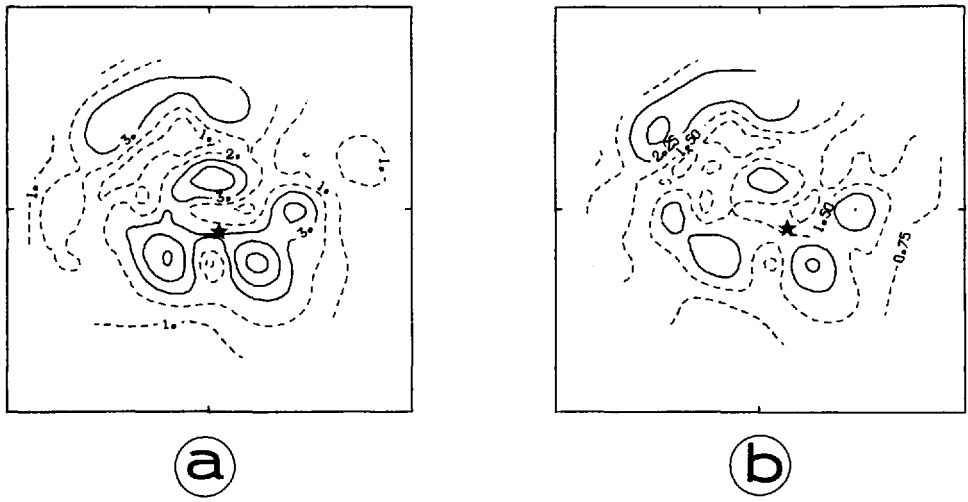

Figure 3. The rate of strain at 850 db (a) and 1000 db (b) for array 3. Multiply by 10^{-6} to give units s^{-1}. The heavy star indicates the eddy center position.

process occurs, through which smaller patches appear, accompanied by erosion of the anomalies. The net result by array 4 is that the salt signature of the original MW tongue is greatly reduced.

The ability of the mesoscale field to deform, and eventually split the original MW patch is illustrated in Figure 3 by the two-dimensional rate of strain $\lambda = [1/4 (V_x + U_y)^2 - U_x V_y]^{1/2}$. This is the rate of elongation of an initially circular water parcel (Batchelor, 1967). Whereas the relative vorticity field, which simply rotates the tracer anomalies, is highest at the eddy center, the rate of strain is maximum at about 30 km from the eddy center. It is there that a significant enhancement of the tracer gradients must be expected (and is observed), causing salt fluxes from the MW patch toward the eddy center, as will be seen in Section 4.

The eddy velocity field is also sheared in the vertical. The main pycnocline being within the depth range of the MW anomalies (700 to 1500 db), we expect the latter to be strongly influenced by the mesoscale vertical shear of horizontal velocity. This is confirmed by curvilinear salinity sections along the axis of the MW patch at the times of the four arrays (Fig. 4). The front of the salinity anomaly which is initially vertical, an indication that in array 1 the MW blob is just entering the domain of influence of the eddy, is then stretched forward at upper levels. By array 4 the splitting of the initial patch is complete, and the salinities of the two newly formed blobs are substantially smaller. As the upper part of the MW patch is drawn forward over fresher water, vertical thermohaline gradients sharpen at its base, which should be a site of preferred mixing since warm salty fluid lies above cold fresh, a situation favorable to the development of salt fingers.

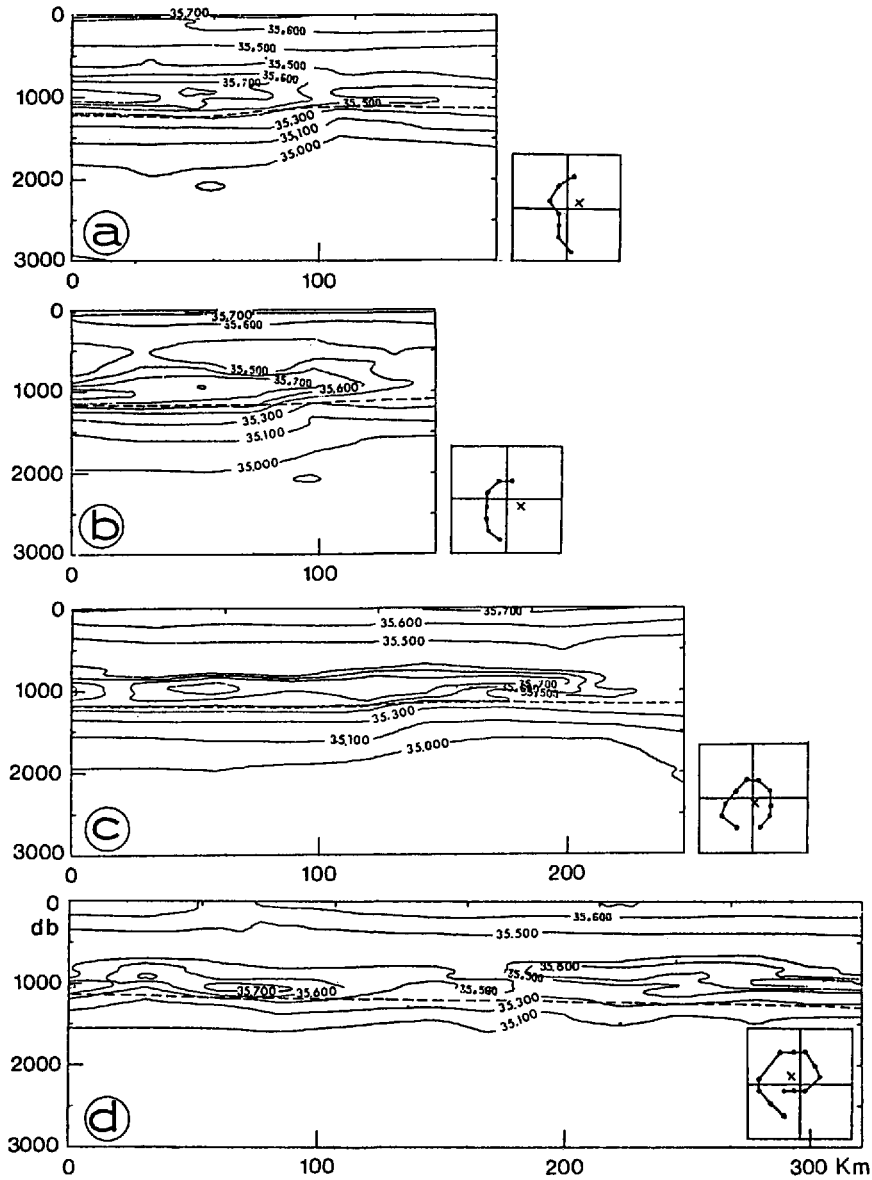

Figure 4. Vertical salinity sections along the MW tongue at the times of the four CTD arrays ((a) to (d)) (from Arhan and Colin de Verdiere, 1985).

c. Small-scale processes. The Tourbillon experiment was not designed to investigate small-scale mixing processes, but strong layering in temperature and salinity profiles were observed at many stations (e.g. Fig. 5a), which is almost certainly indicative of the mixing processes which were occurring. Salinity variance was determined from comparison of filtered and unfiltered profiles (Fig. 5b). The horizontal distribution of

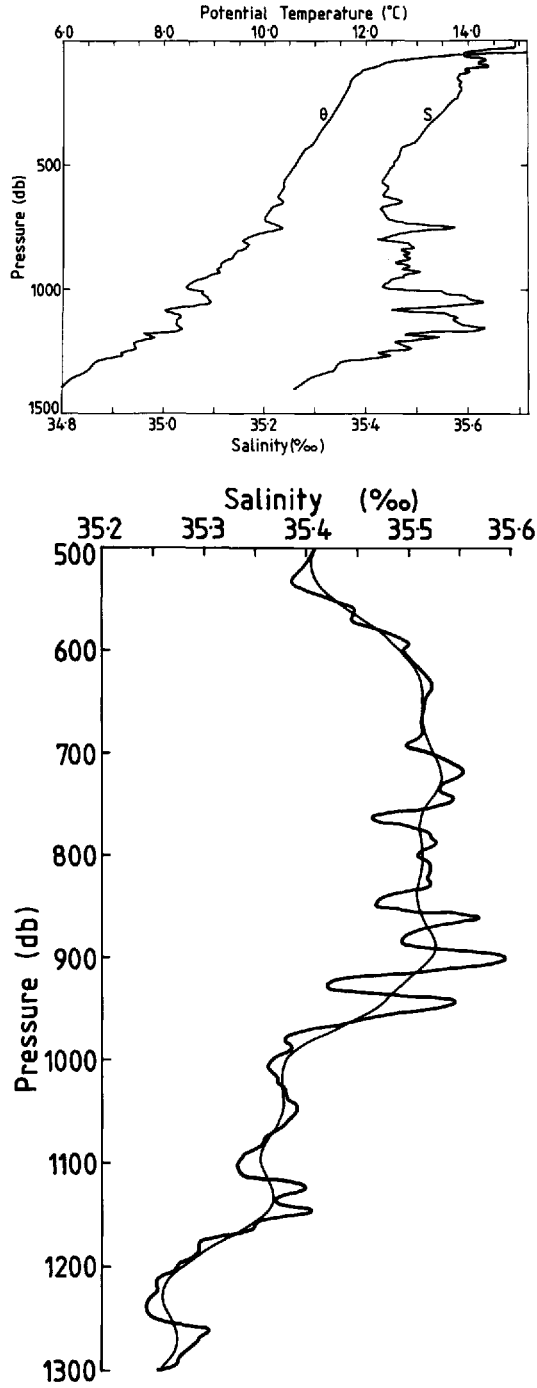

Figure 5. (a) Salinity and potential temperature versus pressure, Station NO 306; (b) Filtered and unfiltered profiles of salinity versus pressure, Station NO 302.

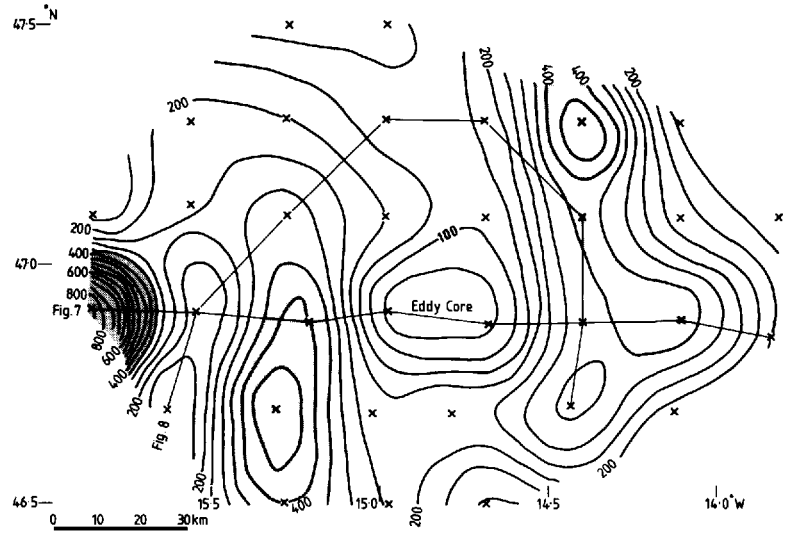

Figure 6. Variance of unfiltered from filtered salinity profiles ($‰^2 \times 10^6$) for the layer 500 to 1500 db in the third array. The axis of the MW Tongue (Fig. 8) and the section used in Figure 7 are also shown.

this variance (Fig. 6) shows that layering is generally most intense on either side of the MW tongue, where thermohaline gradients along isopycnal surfaces are greatest. This layering would appear to be indicative of double diffusively driven intrusions, which have been investigated experimentally by Ruddick and Turner (1979) and theoretically by Toole and Georgi (1981).

d. A mixing scenario. The above observations lead us to a mixing scenario of the large-scale MW anomalies, comparable to that proposed by Garrett (1982). The large-scale salinity gradient in the Tourbillon region is estimated from McDowell's map (Fig. 1) to be about 10^{-6} ‰ m^{-1}. The lateral mesoscale salinity gradient on the density surface $\sigma_1 = 32.0$ (equivalent to McDowell's $\sigma_\theta = 27.6$) in the first Tourbillon array was approximately 10^{-5} ‰ m^{-1} around the MW anomaly. It is clear that a steepening of the gradient had taken place through eddy action. Garrett suggests this steepening to occur in the regions of convergence of a dense eddy field. Because of our limited region of investigation, we have no indication of other eddies being present in the vicinity. We only observe that at the time of array 1 when the MW blob was being caught by the eddy, it seems to have been coming from the southeast, i.e. the direction of the large-scale salinity gradient. Another eddy, meandering of the large-scale gradient, or southeastward movement of the Tourbillon eddy may have brought the salty MW in contact with fresher waters from the northwest. After array 1, teasing out of the MW tongue by the sheared eddy velocity field causes the steepening of thermohaline fronts to continue, so that by array 3 the mesoscale salinity gradient has

reached values around 1.5×10^{-5} ‰ m^{-1}. These values must be high enough for the observed double diffusive frontal intrusions to develop as suggested by Garrett (1982) and Joyce (1977).

In the following the double diffusive interleaving mechanism will be our "small-scale" process. Although it is a very complicated three-dimensional phenomenon, its mixing effects will be simply parameterized by a bulk lateral diffusion coefficient K_{MO}, which we call "frontal mesoscale diffusivity" as it will characterize fluxes through thermohaline mesoscale fronts. From the Tourbillon CTD arrays we will quantify the loss of tracer content from mesoscale water parcels being advected and deformed by the eddy. This will provide an "effective mesoscale diffusivity" K_M, which will be shown to be greater than K_{MO} as a result of shear dispersion. Finally we will use the long-term Tourbillon current-temperature measurements to estimate the "large-scale" horizontal diffusivity K_L, which parameterizes downgradient fluxes caused by the accumulative effects of many mesoscale eddies.

3. Small-scale mixing processes

Ruddick and Turner (1979) and Toole and Georgi (1981) provide expressions enabling the vertical length scale of double-diffusively driven intrusions to be predicted if the salinity and density gradients are known; whereas R & T predict increased length scales if the cross-frontal salinity gradient increases, T & G predict that the dominant vertical scale will decrease. Dominant vertical length scales were not readily identified in most of our profiles, but at station NO 302 (Fig. 5b) there was a well-defined peak at about 40 m in the vertical salinity gradient spectrum. Substitution of values for this station into T & G's model predicts a value of about 70 m, whereas R & T's relationship would predict a value of about 140 m. (Note that lateral salinity gradients are likely to have been underestimated due to the 22 km station spacing, and that larger gradients would bring the prediction from T & G's model nearer to the observed value.)

Strong salt fingering is to be expected on the undersides of warm salty layers when $1 < R_\rho \lesssim 2$, ($R_\rho \equiv \alpha \partial_z T / \beta \, \partial z S$), i.e. $90° > Tu \gtrsim 71.6°$, whilst strong diffusive convection is likely on their upper surfaces when $0.5 \lesssim R_\rho < 1$, i.e. $-71.6° \gtrsim Tu > -90°$, where Tu is the Turner angle, (Schmitt & Georgi, 1982; Ruddick, 1983). We have determined these quantities for successive 10 db layers at each station, and in Figure 7 we show the frequency of occurrence of each of these regimes in a zonal vertical section through the eddy center in the third array. Maximum amounts of MW were encountered at station NO 307 to the west of the eddy center and at station NO 303 to the east. The strong salt fingering regime was most frequent between 1200 and 1700 db (i.e. below the MW tongue), where it was typically found in 60% of the water column; it was also fairly frequent (50%) between 200 and 400 db in the northeast Atlantic Central Water. It was least frequent (25%) between 600 and 1000 db (above the MW tongue) and between 1800 and 2000 db where the influence of Labrador Sea

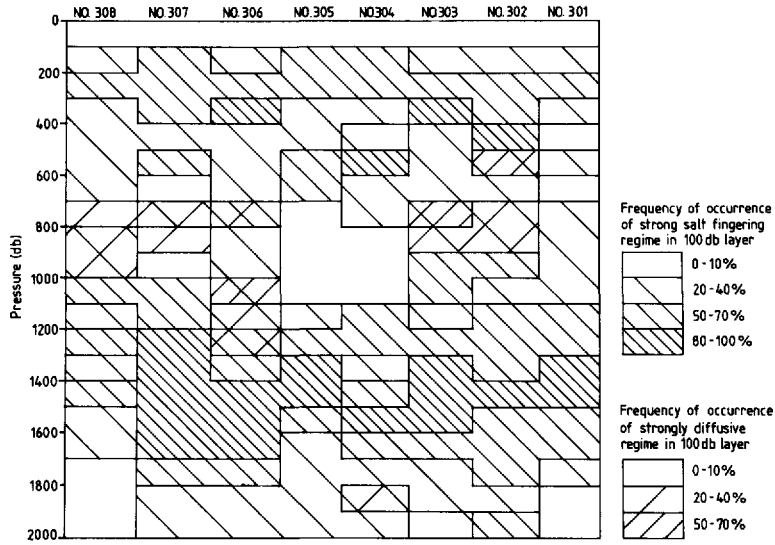

Figure 7. Frequency of occurrence of strong salt fingering and strongly diffusive regimes in a zonal section (NO 308 to NO 301) passing through the eddy core in the third array, (for location of section see Fig. 6).

water has been noted (LGT). The strongly diffusive regime was much less common; the highest frequencies found, which rarely exceeded 30%, were generally between 700 and 1200 db (i.e. within and in the upper part of the MW tongue). Although Figure 7 provides no indication of salt fingering being particularly frequent on either side of the MW tongue, where we invoke it as our basic mixing mechanism, it does show the strongly diffusive regime to be more common in these locations. This is consistent with the presence of warm salty intrusions some tens of meters thick such that salt fingering is confined to the undersides of the intrusions and alternates with regions of strongly diffusive convection where temperature and salinity increase with depth. We found the water to be occasionally statically unstable, on average some two 10 db layers per station; this generally occurred on the underside of the warm salty layers and may be attributable to the heat and salt fluxes associated with salt fingers. It is consistent with the expectation that the vertical fluxes of heat and salt out of the bottom of a warm salty layer due to fingering are greater than those out of the top due to diffusive convection, which will lead to such layers rising relative to isopycnal surfaces. We do see some suggestion of the mesoscale MW tongue rising relative to isopycnals as it encircles the eddy (Fig. 8), but the evidence which we have is far from conclusive; there is appreciable variability in the level at which the tongue occurs, and vertical shear in the flow field will lead to the tongue being stretched laterally into a wedge-like shape, but the upward trend of contours above the maximum concentration may be indicative of real upward movement. Schmitt and Georgi (1982) using fine structure data in a

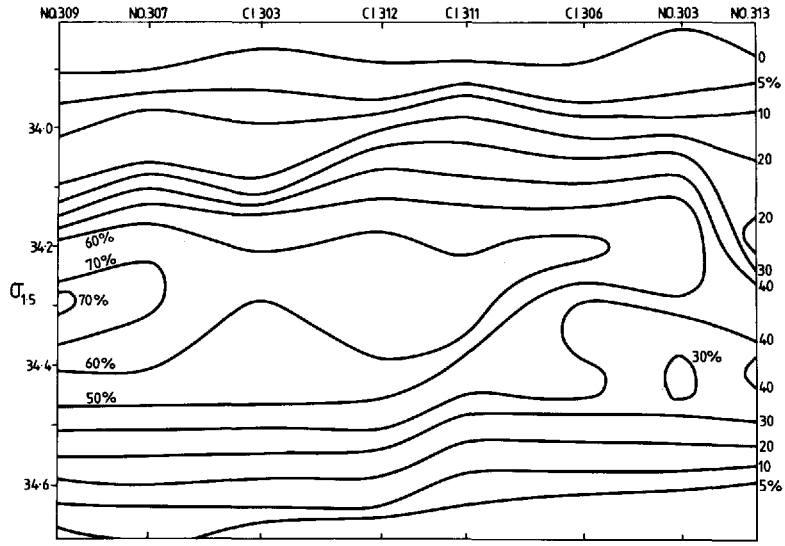

Figure 8. Percentage of MW present in a section along the MW tongue in the third array, (for location of section see Fig. 6).

region of intrusions in the North Atlantic Current estimated effective vertical eddy diffusivities due to salt fingers as about 1×10^{-4} m^2 s^{-1} and, applying this to the Joyce (1977) model of lateral mixing, obtained lateral diffusivities of 5 to 10 m^2 s^{-1} which they stated "should be applicable to cross-frontal water mass transitions with scales of order 5 km." Although this scale is not explicitly resolved by our observations, objective analysis shows the width of the Tourbillon thermohaline fronts to be of order 20 km or less, so that Joyce's model may be reasonably applied. Joyce predicts lateral diffusivity of order $\overline{K_v(\partial\tilde{S}/\partial z)^2}/(\partial S/\partial y)^2$, where K_v, $\tilde{S}$ and $\partial S/\partial y$ are the vertical diffusivity, the interleaving tracer anomaly, and the lateral mesoscale gradient, respectively. Taking $\tilde{S} = S_o \sin(2\pi z/\lambda)$ leads to $\overline{(\partial\tilde{S}/\partial z)^2} \simeq (2\pi/\lambda)^2\,\overline{\tilde{S}^2}$. A mean value of $\overline{\tilde{S}^2}$ characteristic of either sides of the MW tongue is taken from Figure 6 to be $\simeq 3.5 \times 10^{-4}$ (‰)^2. Using $K_v = 10^{-4}$ m^2 s^{-1} for the vertical diffusivity, $\partial S/\partial Y = 1.5 \times 10^{-5}$‰ m^{-1} from Figure 2, and a mean wave-length $\lambda = 40$ m from Figure 5, leads here to a frontal mesoscale diffusivity K_{MO} of order 4 m^2 s^{-1}.

4. Mixing at the mesoscale

The explicitly resolved scale of our observations is from 20 to 200 km. This allows us to quantify the epipycnal loss of tracer content from mesoscale water parcels being advected and deformed by the eddy. Diapycnal mixing will be ignored in our budgeting. This is admittedly a crude simplification of the very complex three-dimensional phenomena evoked previously. Garrett (1982) has argued however that

the fluxes across isopleths of temperature or salinity in a physical situation similar to the one envisioned here are dominated by downgradient epipycnal rather than diapycnal mixing. The mesoscale vertical resolution adopted here is about 200 m, several times the thickness of the interleaving layers. The temperature and salinity profiles were low-pass filtered in the vertical and density computed from the filtered values. Hence in the following we describe mixing along such "coarse" resolution mesoscale isopycnal surfaces. A second simplification is afforded by the fact that the stirring agent, the mesoscale velocity field, is quasigeostrophic. When this is so, the horizontal strain rate exceeds the vertical one by a factor inversely proportional to the small Rossby number. To a good approximation vertical advection terms may be neglected in both the tracer and potential vorticity conservation equations and the stirring-mixing event may be studied in horizontal planes. In the case of temperature and salinity it is possible to be more accurate by describing the event along isopycnal surfaces, but maps of thermohaline fields along horizontal and isopycnal fields showed little difference exemplifying the smallness of vertical motions at the mesoscale.

To summarize, we quantify below the loss of tracer content from the resolved mesoscale (20 to 200 km in the horizontal, 200 m in the vertical) to the next smaller scales along horizontal (or whenever possible isopycnal) surfaces and evaluate crudely the complicated mixing event by a bulk lateral diffusion coefficient.

a. Lagrangian estimations. To obtain estimates of the intensity of mixing along isopycnals of thermohaline anomalies at scales below the oceanic mesoscale, two methods are possible. Either one may use a fixed control volume in space and budget the tracer flux across the outer boundary, the departures from tracer conservation being attributed to mixing, or one may attempt to follow a marked blob of tracer and evaluate the amount of tracer contained in the blob as a function of time. With the data set at hand, we have found it easier to use the second Lagrangian method. An initial approach has been to investigate the evolution of temperature and salinity values (obtained from hydrographic arrays) at the successive positions of the subsurface Tillier acoustic floats which were available. Only one float (No 10) trapped near the center of the eddy conserved accurately its temperature within 0.02°C and salinity within 0.005‰ and indeed a distinct water mass was observed at the eddy core (LGT). Presumably recirculating flows in the core had already homogenized thermohaline gradients there. Other floats demonstrated larger variations of temperature (0.4°C) and salinity (0.1‰), particularly those near to the MW tongue. Such single point estimates are clearly unsatisfactory, and this suggests a more integrated method. Using both current meter and float data it is possible to construct daily optimal streamfunction charts at 700 and 1500 m. After nonlinear interpolations using only the velocity data from these two levels, the velocity field at 1000 m can be used to estimate the deformation of an arbitrarily chosen patch delimited by a given "material line." The integration of salt and temperature anomalies within these lines is then possible at

the times of the hydrographic arrays. Along isopycnal surfaces, we estimate the diffusivity coefficient from the following relation:

$$\frac{\partial}{\partial t}\iint_D CdA = K_M \oint_{\partial D} \nabla C \cdot \mathbf{n}\, dl \tag{1}$$

where D is the area enclosed by a given material line, ∂D, and C is tracer concentration. This relation requires the knowledge of the evolution of ∂D along isopycnals. What we have at our disposal to compute that evolution is a smoothed velocity field at a given depth. As indicated earlier the velocity fields along horizontal and isopycnal surfaces should not depart drastically from each other provided the Rossby number is small. At any rate, this is the best we can achieve (and will probably be so for a long time). The evaluation of (1) is straightforward: the quantity of tracer contained within a circular material line ∂D is calculated at the time of a given hydrographic array using optimal maps of salinity, temperature, or potential vorticity. Using the daily optimal velocity fields, the deformed material line D' and the salt (or heat) content within D' can be determined at each successive array (roughly 2 weeks apart). Hence we estimate K_M from (1) as:

$$K_M = \frac{1}{\Delta t}\frac{\iint_{D'} CdA - \iint_D CdA}{\oint_{\partial D} \nabla C\, \mathbf{n}\, dl} \tag{2}$$

For illustrative purposes, we show in Figure 9, the material lines and the computed trajectories of fluid parcels at 1000 m.

A discussion of the errors is critical, for any uncertainties in these trajectories produce artificial diffusion. Differences between horizontal and isopycnal surfaces at 1000 m lead to velocity errors of order 1 cm s^{-1}, the rms isopycnal displacement (35 m) times the rms vertical shear (2.5×10^{-4} s^{-1}). The biggest contribution however comes from vertical and horizontal interpolation errors between velocity data points. The rms velocity signal being 7 cm s^{-1}, 2 cm s^{-1} sampling errors are not unlikely. To these we must add instrumental errors (1 cm s^{-1}). In the face of these random velocity errors, ϵ_u(~3 cm s^{-1}), it would seem that the evaluation of K_M is hopeless. We think, however, that both time integration of the trajectories and spatial averaging inside a material line can lead to substantial error reductions. If T_e is the integral time scale of the ϵ_u field, a random walk for a time Δt large compared to T_e leads to position errors ϵ_r given by:

$$\epsilon_r \simeq \epsilon_u (T_e\, \Delta t)^{1/2}$$

If L_D is the size of the domain D of integrations, the relative precision of K_M is then of order ϵ_r / L_D as can be seen from Eq. 2.

Of course, this error estimate depends on unknown quantities such as the time scale

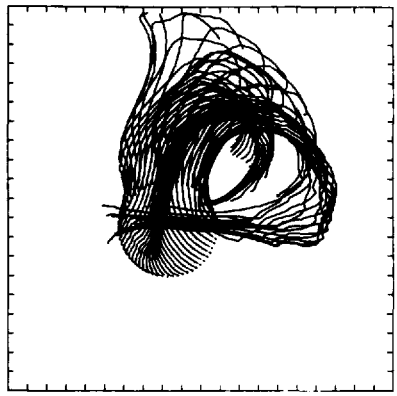

a.

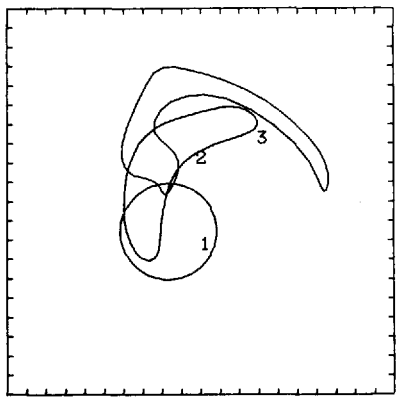

b.

Figure 9. (a) The trajectories of fluid parcels lying initially on a circle at 1000 m depth for 56 days; (b) The material lines 10 days apart constructed from the trajectories. Tick marks represent 10 km.

of the velocity errors. The Lagrangian integral time scale of the velocity is of the order of 2 days (Mercier and Colin de Verdiere, 1985). If we decide to identify the time scales of the errors with the scales of the velocity itself, then the precision on the diffusivity estimate is of the order of 30% for arrays 2 weeks apart (Δt = 2 weeks, T_e = 2 days, L_D = 50 km, ϵ_u = 3 cm s^{-1}). A more pessimistic choice may lead to a larger time scale for the velocity errors: for T_e of order Δt the position errors ϵ_r now grow as $\epsilon_u \Delta t$ reaching the size of the domain of integration L_D after about 2 weeks and degrading the precision to more than 100%.

Choosing for the boundary ∂D an initial circular line of 25 km radius (r) located in the forward part of the MW tongue, Table 1 shows the computation of K_M from Eq. 2

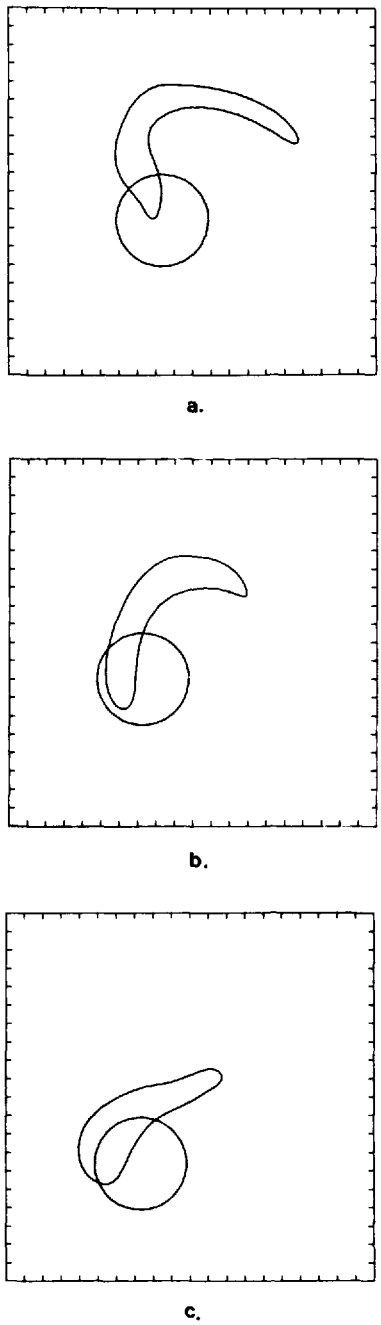

Figure 10. Deformation of a material circle between respectively array 1 and 2 (a), array 2 and 3 (b), and array 3–4 (c). The properties were integrated inside these contours to estimate the diffusivity coefficient K_M. Tick marks represent 10 km.

Table 1. Lagrangian estimations of K_M.

	$(1) = \frac{r\,\delta C}{2\,\Delta t}$	$(2) = \frac{\Delta C}{\Delta X}$ (normal)	$K_M = \frac{(1)}{(2)}$
Temperature	$m\,s^{-1}\,°C$	$(°C\,m^{-1})$	$m^2\,s^{-1}$
Array 1–2	-2.8×10^{-3}	-2.3×10^{-5}	122
Array 2–3	-2.6×10^{-3}	-3.0×10^{-5}	87
Array 3–4	-5.0×10^{-3}	-2.0×10^{-5}	250
Salinity	$m\,s^{-1}\,‰$	$(‰\,m^{-1})$	$m^2\,s^{-1}$
Array 1–2	-7.6×10^{-4}	-3.8×10^{-6}	200
Array 2–3	-3.6×10^{-4}	-7.7×10^{-6}	47
Array 3–4	-1.2×10^{-3}	-4.6×10^{-6}	260
Potential Vorticity	(1) $rad\,s^{-2}$	(2) $m^{-2}\,rad\,s^{-1}$	$m^2\,s^{-1}$
Array 1–2	9.5×10^{-8}	5.7×10^{-10}	168
Array 2–3	5.1×10^{-9}	5.9×10^{-10}	10
Array 3–4	2.2×10^{-8}	1.29×10^{-10}	178

at 1000 m, and Figure 10 illustrates the deformations of the material lines between arrays.

In the above r (=25 km) is the radius of the initial circular contour and Δx (=13 km) is the grid size over which the averaged normal gradient $\Delta C/\Delta x$ is calculated. Lateral salinity gradients reported here are somewhat smaller than those quoted in the previous paragraphs (of order $10^{-5}‰\ m^{-1}$) because they are averages over closed contours, whereas the former were characteristic of a direction perpendicular to the MW tongue axis. Note that the heat, salt and potential vorticity fluxes are down-gradient for all estimates. Although the error calculations are somewhat arbitrary this result gives confidence in the order of magnitude of the positive diffusivity K_M.

In other instances Arhan and Colin de Verdiere (1985) have shown that potential vorticity can be conserved quite well. This is not necessarily in contradiction with the present results. The transfer of potential vorticity to smaller scales and its ultimate mixing depends crucially upon the local strain rate which varies markedly across the field as shown in Figure 3. When it is small the conservation of the tracer may be excellent.

We do not consider that the variations of K_M within Table 1 justify interpretation and conclude only that the mixing of thermohaline anomalies and potential vorticity occurs with a positive diffusivity coefficient of order $10^2\ m^2\,s^{-1}$.

b. The shell model. The fundamental assumption in the following independent, but also Lagrangian, estimation of K_M is that the eddy is sufficiently strong to trap recirculating water parcels and hence tracer anomalies, so that changes in water mass properties within concentric shells moving bodily with the eddy can be attributed to

mixing. A direct illustration was provided at the eddy core by a subsurface float trapped there for about 40 days (LGT, 1983).

The salinity distribution within the density range $31.86 < \sigma_1 < 32.06$ (e.g. Fig. 2b) has led to a model of the eddy with a series of shells of different salinity characteristics around a core of constant salinity; these shells may be attributed to the successive entrainment of different waters encountered by the eddy in previous months. This concentric shell model is illustrated in Figure 11 which shows the radii of the successive shell boundaries and the number of stations sampling each part during each of the four arrays. Note that, particularly in the outer shell, these stations were not distributed uniformly due to the position of the moving eddy relative to the fixed station array. The inner shell appeared to include the region of largest rate of strain (Fig. 3). Whereas the salinity of the eddy core within this density range remained virtually constant during the four arrays (Fig. 12), the salinity of the inner shell increased from 35.42‰ (less than that of the core) in the first array to 35.52‰ in the fourth array. The outer shell comprises the MW tongue and was more saline than the inner shell during the first three arrays, but decreased to the same value as the inner shell in the fourth array; the

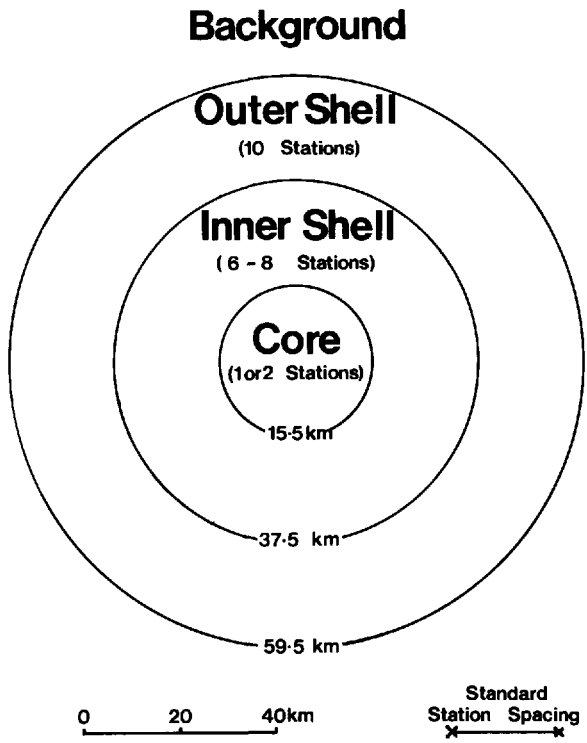

Figure 11. A concentric shell model for the Tourbillon eddy.

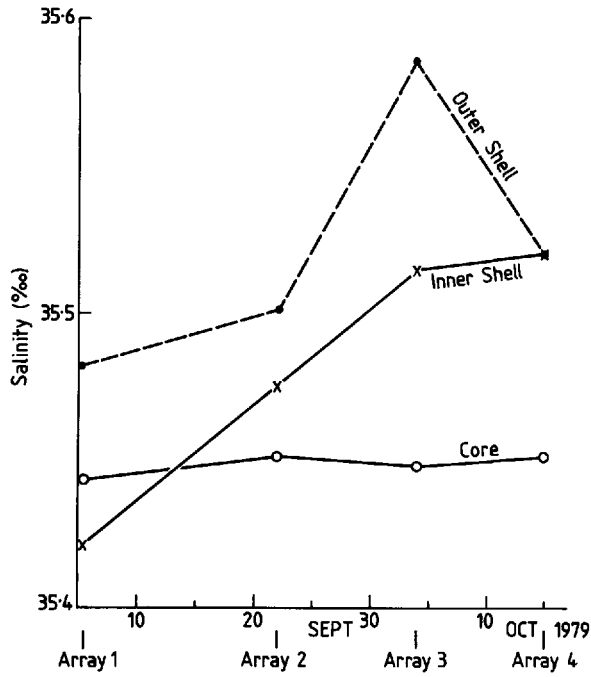

Figure 12. Mean salinities in the density range $31.86 < \sigma_t < 32.06$ versus time for the eddy core, the inner shell and the outer shell.

increase in its salinity from the first to the third array is attributable to the MW tongue extending further round the eddy rather than to an increase in the salinity values in the tongue. Attributing the increase in salinity of the inner shell to mixing between this shell and the outer shell leads to an estimate of the value of K_M. Taking the change of salinity of the inner shell to be 0.1‰ in 40 days leads to a mean salt flux across its outer boundary of 4.5×10^{-4} kg m^{-2} s^{-1}.

Equating this flux to $-K_M \rho \, \partial s/\partial r$ and taking $\partial s/\partial r$ between the inner and outer shells to be 0.05‰/22 km = 2.3×10^{-6}‰ m^{-1} (averaged value along the boundary of the inner shell), $\rho = 10^3$ kg m^{-3}, gives $K_M \simeq 2 \times 10^2$ m^2 s^{-1}.

c. Water mass estimations. Quantitative estimates have been made of the mass of MW with θ-S properties 10°C, 36‰ assumed to have mixed with ENAW (Harvey, 1982) within the layer 500–2000 db at each of the Tourbillon array stations (Harvey and Glynn, 1985). Whereas the mean value per station remained almost constant during the time of the whole intensive experiment (Fig. 13), the variance about this mean decreased markedly from the first array through to the fourth. If this is taken to indicate that during the experiment the total mass of MW within the layer 500–2000 db and within the station array was approximately conserved, but was mixed with adjacent water so that peak concentrations decreased and became spread over a wider

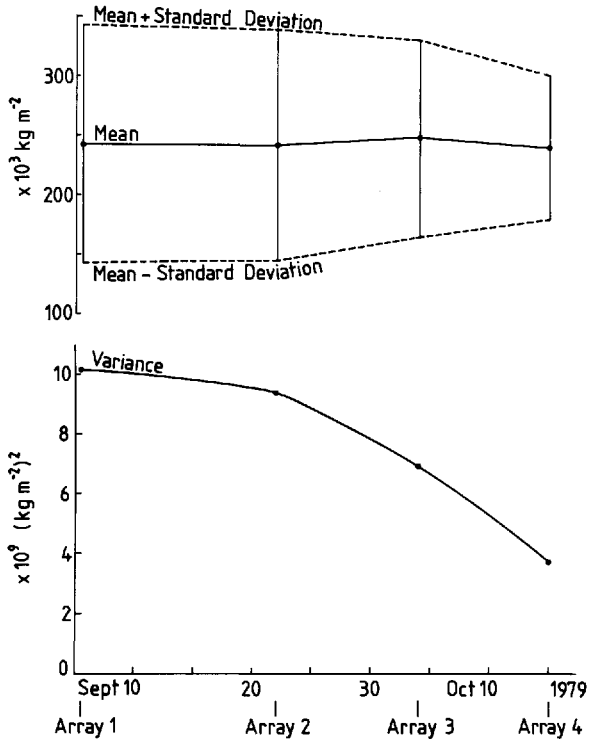

Figure 13. Mean mass of MW and its variance in the layer 500 to 2000 db for each of the four CTD arrays.

area, the MW can be used in the same way as a dye patch to estimate K_M. It has been assumed that a particular background value of MW was present at all stations, and the radially symmetric equation for isotropic diffusion in the horizontal plane has been used.

The procedure was to determine the equivalent circular areas for given concentrations (C) above the background value selected (Co) for each array and to then compute the radially symmetrical variance σ_{rc}^2 defined as

$$\sigma_{rc}^2 = \left[\int_o^\infty r^2 (C - Co)\, 2\pi r\, dr\right]\left[\int_0^\infty (C - Co)\, 2\pi r\, dr\right]^{-1}.$$

From this the diffusion coefficient $K_m = \frac{1}{4}\, \partial\sigma_{rc}^2/\partial t$ was determined between successive arrays and between the first and fourth array. The results obtained are set out in Table 2 for three different values of Co, from which it would appear that a reasonable estimate for K_m would be $0.44\ (\pm 0.16) \times 10^2\ \mathrm{m^2\ s^{-1}}$.

d. Discussion. Values of the lateral mixing coefficient K_M obtained in Section 4 a, b, c, are surprisingly large compared with the mesoscale diffusivity K_{MO} inferred in

Table 2. Diffusion coefficients obtained from the four arrays. Units for C_o: 10^3 kg m^{-2}; for σ_{rc}^2: 10^7 m^2; for K: m^2 s^{-1}.

C_o		Array 1	Array 2	Array 3	Array 4	Mean, Array 1–Array 4
160	σ_{rc}^2	126	138	165	181	
	K	22	66	43		41
170	σ_{rc}^2	108	129	154	167	
	K	38	60	34		44
180	σ_{rc}^2	96	119	141	152	
	K	42	53	29		42

paragraph 3 from Joyce's model. Comparisons with theory and numerical calculations help to clear up this dilemma.

Studying the homogenization of a tracer in flows with closed streamlines, Rhines and Young (1983) distinguish two stages: the tracer is first rapidly diffused along streamlines with a shear augmented diffusivity increasing with time as t^2, whereas dispersion across streamlines occurs over a longer time period. The first "averaging phase" takes a time of order $T_a = P_e^{1/3} L/U$, where the Peclet number $P_e = UL/K$ for a flow of characteristic length and velocity L and U is based upon the explicit diffusivity K. Considering that in our observations $K_{MO} \simeq 4$ m^2 s^{-1} is the basic explicit lateral diffusivity, that L and U are respectively equal to 30 km (zero crossing of the transverse velocity correlation function) and 7 cm s^{-1} (rms velocity at 1000 m), we find $P_e \simeq 500$ and an "averaging time" $T_a \simeq 40$ days. Considering the MW to have just entered the eddy domain of influence at the beginning of the 40-day intensive experiment, we may take our observations to approximately cover the averaging phase. Rhines and Young describe that period itself as being first dominated by sheared advection of the anomalies, diffusion becoming effective at the very end and causing a sudden destruction of the orginal Fourier component. This description may well be applied to the behavior of the MW tongue, discussed in Section 2b, the diffusion regime overriding the advection regime after array 3. This evolution is also illustrated by the spatial covariances for both density and salinity along the isopycnal surface $\sigma_1 = 32.0$, computed at the times of the four arrays and shown in Figure 14. As already noted by LGT, the variance of the salinity signal decreased more rapidly than that of density during the four arrays an indication that mixing along isopycnals was occurring. However, the salinity covariances also reveal that, whereas the signal level appears relatively stable from array 1 to 3, its horizontal scale (identified with the zero crossing) decreased rapidly from about 55 to 20 km. This confirms that an efficient transfer of the salinity spectrum toward smaller scales was occurring under the effect of shear advection. After this stirring phase, mixing occurred and the salinity variance fell off rapidly as can be seen between arrays 3 and 4. By array 4 the salinity field correlation scale was less than our normal grid spacing of 22 km.

Looking back at how our mesoscale diffusivities K_M were estimated, a proper

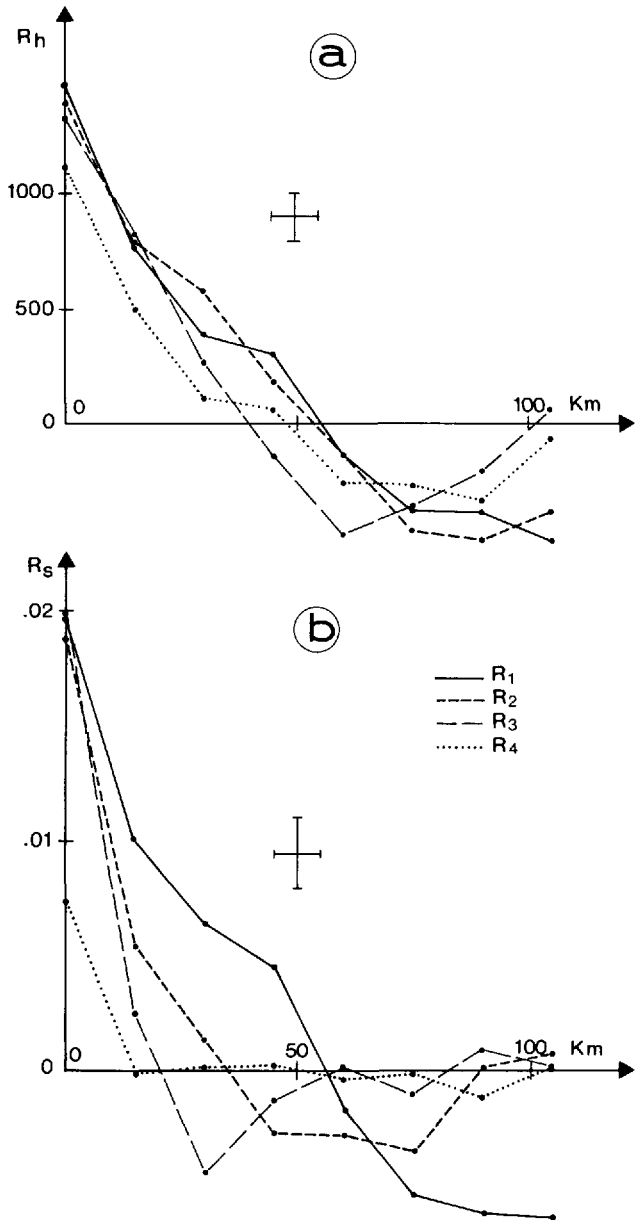

Figure 14. (a) Spatial correlation R_h of the topography of the isopycnal surface $\sigma_1 = 32.0$ (Units in $(db)^2$). (b) Spatial correlation R_s of salinity along the isopycnal surface $\sigma_1 = 32.0$ (Units in $(‰)^2$). The correlations corresponding to the four CTD arrays (R1 to R4) are shown along with a rough estimation of the error bars.

interpretation for that parameter is then that of an effective shear augmented diffusivity, the underlying explicit diffusivity associated with the smaller scale processes being K_{MO}. The analytical results predict that the explicit diffusivity should be multiplied by $P_e^{2/3}$ to get the shear enhanced diffusivity along streamlines at time T_a. For the present observations that ratio would be about 65, whereas our order of magnitude for K_M/K_{MO} is about 25. This is consistent with our K_M being representative of mixing both along and across streamlines, and averaged over the timelag separating two arrays.

Numerical experiments by Haidvogel and Keffer (1984) confirm this shear enhanced aspect of K_M. A spot of tracer was released in a periodic barotropic quasigeostrophic model containing a rich distribution of random eddies. They carried out several realizations of such releases and computed the diffusivity as the time derivative of the moment of inertia of the tracer distributions. They found this diffusivity to be larger by a factor of about 30 than the explicit diffusivity that they imposed, a value even closer to our present experimental results. Furthermore, their simulations (see their Fig. 16) exhibit a slowly time-increasing diffusivity reminiscent of the analytical results quoted above. Our K_M estimations are too crude to show this accelerating tendency of the effective diffusivity but comparisons with the model again support the idea that what we have estimated is a shear-augmented or effective diffusivity.

5. Large-scale speculations

a. Interpretation of heat fluxes. The previous analysis of what appears to be one event may be considered in a more general context. The 8-month velocity and temperature time series available allowed the low passed (cut-off at 2 days) eddy heat fluxes to be computed, (LGT), averaged over the Tourbillon area (6 or 7 moorings). Although the standard errors of these heat fluxes are of the order of the values themselves, the northwestward direction of the flux vector stands out (see Table 3). It appears to be oriented parallel to the large-scale salinity gradient mapped by McDowell (Fig. 1) which we consider to be significant. We assume as a working hypothesis that these heat fluxes are to a large extent compensated by opposing salt fluxes so as to lead to negligible buoyancy fluxes. The 2-month intensive experiment suggests this idea, although compensation is not quite complete below 1000 m where the temperature signal overrides that of salinity. Such a hypothesis leads to salt fluxes given by:

$$\langle S'\mathbf{u}'\rangle \sim \frac{\alpha}{\beta}\langle \mathbf{u}'T'\rangle$$

where α ($\sim 1.8 \times 10^{-4}$°C^{-1}) and β ($\sim 7.5 \times 10^{-4}$) are the coefficients of thermal and salt (salinity units ‰) expansion respectively. From the above table $\langle u'T'\rangle$ is typically 2×10^{-3} m s^{-1}°C which leads to salinity fluxes of order 4.8×10^{-4} m s^{-1} at 1000 m. If

Table 3. Eddy heat fluxes (m s^{-1} °C).

depth (m)	$\langle u'T' \rangle$	$\langle v'T' \rangle$
700	-3.0×10^{-3}	1.2×10^{-3}
1500	-1.1×10^{-3}	1.6×10^{-3}
1100	-4.0×10^{-3}	2.0×10^{-3} (one mooring only)

the equivalence between time and spatial averaging is accepted, the salinity fluxes derived from velocity-temperature correlations represent averages over several eddy diameters and must be properly interpreted as fluxes from the large-scale permanent salinity fields. This, together with a large-scale salinity gradient at the Tourbillon site of 10^{-6}‰ m^{-1} (from McDowell's chart), implies large-scale diffusivities K_L of order 500 $m^2 s^{-1}$, somewhat higher than the 0 (100 $m^2 s^{-1}$) effective mesoscale diffusivities estimated previously. Kuo and Veronis (1973) used a comparable value (600 $m^2 s^{-1}$) to model the large-scale distribution of oxygen. What dictates the relative magnitude of K_L and K_M? Invoking previously the analytical results of Rhines and Young, we found that the shear augmented diffusivity along streamlines at time $T_a = L/U\,Pe^{1/3}$ is of the order $K_{MO}\,P_e^{2/3}$, which may be called the "maximum mesoscale" diffusivity, and denoted K_{M1}. Parameterizing the Reynolds fluxes from the large scale to the mesoscale in terms of a bulk diffusivity now leads to $K_{L1} = UL$ as a proper scale for K_L, so that K_{L1}/K_{M1} is of order $Pe^{1/3}$, i.e. weakly dependent on the value of the Peclet number. With the parameters characteristic of the Tourbillon intensive experiment ($Pe = 500$), we have $K_{L1} \simeq 2100$ $m^2 s^{-1}$, $K_{M1} \simeq 260$ $m^2 s^{-1}$, their ratio being about 8. We argued that our K_M ($\simeq 100$ $m^2 s^{-1}$) was smaller than K_{M1} because it was representative of transverse as well as longitudinal mixing, and was estimated previous to T_a. Now we suggest that finding $K_L \simeq 500$ $m^2 s^{-1}$, i.e. only one fourth of K_{L1}, is an indication that the mesoscale activity in the Tourbillon area cannot be simply viewed as a continuous succession of such events as the intense eddy observed in September–October 1979. Examination of the 8-month time series presented by LGT confirms that interpretation: after the first two months of the intensive experiment, the Tourbillon area was free of any eddy activity for four months, after which a second eddy was observed, and henceforth intermittency of eddy passages would then explain the lower observed K_L and the relative closeness between K_L and K_M. This line of thought strongly suggests the mixing mechanisms described above to be major contributors to the estimated Reynolds fluxes.

b. Maintenance of the large-scale salinity field. The ubiquitous MW signal in the North Atlantic has aroused the interest of many oceanographers. Needler and Heath (1975) used an advection-diffusion equation in the vertical plane to estimate the ratio of horizontal (and vertical) diffusion coefficients to advective speed necessary to

reproduce the large-scale MW distribution. Richardson and Mooney (1975) demonstrated that given sufficient diffusion a MW anomaly could penetrate westward across the subtropical gyre.

Both the strength and the direction of the eddy salt fluxes inferred above from the measured heat fluxes suggest their role in maintaining the large-scale distribution of the salinity field. Whether these fluxes estimated at a particular place and time are consistent with the maintenance of the large-scale salinity field is checked in the following.

The large-scale salt distribution results from a balance between advection, fluxes to smaller scales, and the source at Gibraltar:

$$\langle \mathbf{U}_H \rangle \nabla \langle S \rangle + \nabla \cdot \langle S' \mathbf{U}'_H \rangle = \text{Source}. \tag{3}$$

Because vertical advection terms are not represented, (3) should be seen as a vertical integration of the complete conservation equation over a depth interval H at which the vertical fluxes vanish. Practically, H is loosely defined here as the thickness of the layer of MW influence. Furthermore it is more appropriate to view the above in coordinates defined along mean isopycnal rather than horizontal surfaces. The bracketed average operation refers to a spatial average over a horizontal scale larger than the mesoscale yet smaller than the scale of the MW plume itself. We do not know the divergence of the salt fluxes, but we can integrate (3) over a domain bounded by a particular contour Γ along which the salinity is constant ($\langle S \rangle = \langle S_o \rangle$). We obtain after transformation:

$$\langle S_o \rangle \oint_\Gamma \langle \mathbf{u}_H \rangle \, \mathbf{n} \, dl + \oint_\Gamma \langle s' \mathbf{u}' \rangle \, \mathbf{n} \, dl = \iint_A \text{source} \, dA \tag{4}$$

in which $\mathbf{n}$ is the unit normal to the contour Γ. The first term in (4) represents the net mass flux across the contour and must vanish (ignoring flow through the straits of Gibraltar) on account of the horizontal nondivergence of the large-scale field. Hence if the length of the mean contour $\langle S_o \rangle$ is denoted L_o (4) tells us that the following order of magnitude balance must hold:

$$H \, L_o \, \langle s'u' \rangle \sim \delta S \, V \tag{5}$$

in which δS is the anomaly of salinity at Gibraltar above the background salinity of surrounding waters and V the volume transport of the Mediterranean outflow.

Appropriate values for V can be found in the literature, e.g. Zenk (1975) gives 1×10^6 m^3 s^{-1} at a salinity of 38.4‰. The background salinity of the water in the absence of the MW outflow would be about 35.4‰ yielding a net anomaly $\delta S \sim 3$‰. Although we have obtained a pointwise estimation of the salt flux, the length L_o of a given mean salinity contour remains elusive. If L_o is estimated from McDowell's 35.6‰ smoothed contour which passes through the Tourbillon area, it is about 4000 km. With this value, the turbulent salt flux as estimated in Section 5a to be 4.8×10^{-4} m s^{-1}, and H as 1000 m, the *LHS* of (5) becomes about 2×10^6 m^3 s^{-1} while the *RHS* is 3×10^6 m^3 s^{-1}.

These two values are comparable, suggesting our Reynolds fluxes to be representative of the eastern North Atlantic, and the mixing events observed in Tourbillon to be relevant for the maintenace of the large-scale salt distribution of Mediterranean origin.

6. Conclusion

The Tourbillon experiment has provided some unexpected and unique (but, of course, incomplete) observations of the successive processes contributing to the lateral mixing of large-scale thermohaline anomalies. The tracer maps from the four successive CTD arrays illustrate the stirring and sharpening of the large scale thermohaline gradient by a mesoscale velocity field. Interleaving is observed at the sharp fronts thus generated, which, associated with double diffusion, is likely to provide the basic mixing mechanism. Using the velocity-temperature time series, this scenario, although occurring intermittently at a given location, has been shown to be able to provide lateral salt fluxes of the correct order of magnitude to maintain the large-scale salt distribution of Mediterranean origin.

The underlying explicit lateral diffusivity K_{MO} has been inferred from Joyce's model to be about 4 $m^2\ s^{-1}$. Several approaches have led to values of the effective shear augmented mesoscale diffusivity K_M of order 100 $m^2\ s^{-1}$. Although taken individually each of these K_M computations may appear weak, due to their associated uncertainties, their similarity gives confidence that they provide the correct order of magnitude. Finally, the large-scale diffusivitiy K_L was estimated at about 500 $m^2\ s^{-1}$. Consistency between K_{MO}, K_M and K_L was verified using the Rhines and Young model of tracer mixing in horizontal shear flows.

It is, of course, difficult to generalize our findings to other areas. The mixing processes described herein depend crucially upon double diffusive convection acting at the interfaces of the interleaving layers.

Because a potential vorticity signal was associated with the thermohaline signal, the same mixing coefficients were shown to apply to potential vorticity. A passive geochemical tracer would be mixed similarly to the thermohaline anomalies in the present area, but of course at different rates in regions devoid of thermohaline fronts, where double diffusive processes are not active.

Acknowledgments. M. Arhan and A. Colin de Verdiere were supported in this investigation by IFREMER (Grant 152400); the participation of J. G. Harvey was supported by the Natural Environment Research Council (Grants GR3/4143 and 5145).

REFERENCES

Arhan, M. and A. Colin de Verdiere. 1985. Dynamics of eddy motions in the eastern North Atlantic. J. Phys. Oceanogr., *15*, 153–170.

Batchelor, G. K. 1959. Small scale variations of convected quantities like temperature in a turbulent field. J. Fluid Mech. *5*, 113–133.

—— 1967. An Introduction to Fluid Dynamics. Cambridge University Press, 615 pp.
Garrett, C. 1982. On the parameterization of diapycnal fluxes due to double-diffusive intrusions. J. Phys. Oceanogr., *12,* 952–959.
Haidvogel, D. B. and T. Keffer. 1984. Tracer dispersal by mid-ocean mesoscale eddies. Part 1: Ensemble Statistics. Dyn. Atmos. Oceans, *8,* 1–40.
Harvey, J. 1982. θ-S relationships and water masses in the eastern North Atlantic. Deep-Sea Res., *29,* 1021–1033.
Harvey, J. and S. Glynn. 1985. Water mass structure and transport in the Tourbillon eddy. Deep-Sea Res., *32,* 675–695.
Joyce, T. M. 1977. A note on the lateral mixing of water masses. J. Phys. Oceanogr., *7,* 626–629.
Kuo, H. H. and G. Veronis. 1973. The use of oxygen as a test for an abyssal circulation model. Deep-Sea Res., *20,* 871–888.
Le Groupe Tourbillon. 1983. The Tourbillon experiment: a study of a mesoscale eddy in the eastern North Atlantic. Deep-Sea Res., *30,* 475–511.
McDowell, S. E. 1982. Isopycnal hydrography and mixing of North Atlantic intermediate waters. Ph.D. thesis, University of Rhode Island, Narragansett, RI, 227 pp.
Mercier, H. and A. Colin de Verdiere. 1985. Space and time scales of mesoscale motions in the eastern North Atlantic. J. Phys. Oceanogr., *15,* 171–183.
Needler, G. T. and R. A. Heath. 1975. Diffusion coefficients calculated from the Mediterranean salinity anomaly in the North Atlantic Ocean. J. Phys. Oceanogr., *5,* 173–182.
Okubo, A. 1967. The effect of shear in an oscillatory current on horizontal diffusion from an instantaneous source. Int. J. Oceanol. Limnol., *1,* 194–204.
Rhines, P. B. and R. W. Young. 1983. How rapidly is a passive scalar mixed within closed streamlines? J. Fluid Mech. *133,* 133–145.
Richardson, P. L. and K. Mooney. 1975. The Mediterranean outflow—a simple advective—diffusive model. J. Phys. Oceanogr., *5,* 476–482.
Ruddick, B. R. 1983. A practical indicator of the stability of the water column to double-diffusive activity. Deep-Sea Res., *30,* 1105–1107.
Ruddick, B. R. and J. S. Turner. 1979. The vertical length scale of double-diffusive intrusions. Deep-Sea Res., *26,* 903–913.
Schmitt, R. W. and D. T. Georgi. 1982. Finestructure and microstructure in the North Atlantic Current. J. Mar. Res., *40* (Suppl.), 659–705.
Toole, J. M. and D. T. Georgi. 1981. On the dynamics and effects of double-diffusively driven intrusions. Prog. in Oceanogr., *10,* 123–145.
Zenk, W. 1975. On the Mediterranean outflow west of Gibraltar. "Meteor" Forsch-Ergebn. A, *16,* 23–34.

Received: *19 June, 1984;* revised: *25 November, 1985.*